*J. Fluid Mech.* (1999), *vol.* 398, *pp.* 299–319. Printed in the United Kingdom



# Miscible displacement in a Hele-Shaw cell at high rates

By E. LAJEUNESSE[1], J. MARTIN[1], N. RAKOTOMALALA[1], D. SALIN[1] AND Y. C. YORTSOS[2]

[1]Laboratoire FAST, Bâtiment 502, Campus Universitaire, F-91405 Orsay Cedex, France†

[2]Department of Chemical Engineering, University of Southern California, Los Angeles, CA 90089-1211, USA

(Received 7 December 1998 and in revised form 21 June 1999)

We study experimentally and theoretically the downward vertical displacement of one miscible fluid by another lighter one in the gap of a Hele-Shaw cell at sufficiently high velocities for diffusive effects to be negligible. Under certain conditions on the viscosity ratio, $M$, and the normalized flow rate, $U$, this results in the formation of a two-dimensional tongue of the injected fluid, which is symmetric with respect to the midplane. Thresholds in flow rate and viscosity ratio exist above which the two-dimensional flow destabilizes, giving rise to a three-dimensional pattern. We describe in detail the two-dimensional regime using a kinematic wave theory similar to Yang & Yortsos (1997) and we delineate in the $(M, U)$-plane three different domains, characterized respectively by the absence of a shock, the presence of an internal shock and the presence of a frontal shock. Theoretical and experimental results are compared and found to be in good agreement for the first two domains, but not for the third domain, where the frontal shock is not of the contact type. An analogous treatment is also applied to the case of axisymmetric displacement in a cylindrical tube.

## 1. Introduction

Fluid flow and fluid displacements in a Hele-Shaw cell (of length $L$, width $W$ and thickness $b$, with $L > W \gg b$) have been the subject of many theoretical and experimental investigations in the past (McCloud & Maher 1995 and references therein). Under single-phase viscous flow conditions, the transverse averaging of the flow variables across the gap of the cell leads to Darcy's law, where the velocity is proportional to the pressure gradient. The resulting analogy to flows in homogeneous porous media (Homsy 1987) and, more generally, to two-dimensional potential flows has been extensively exploited. Of particular interest has been the viscous fingering instability that takes place when a less viscous fluid displaces a more viscous one in an immiscible displacement. Under conditions such that a well-defined meniscus in the gap (the $L \times b$ plane) separates the two fluids, the fully developed state is the well-known Saffman–Taylor finger in the $L \times W$ plane (Saffman & Taylor 1958). The geometrical characteristics of this finger have been well described using a two-dimensional potential flow approach. The two-dimensional approach is valid only

† Laboratoire FAST (Fluides, Automatique et Systèmes Thermiques) is associated with CNRS and with Universités Paris VI et XI (UMR 7608).

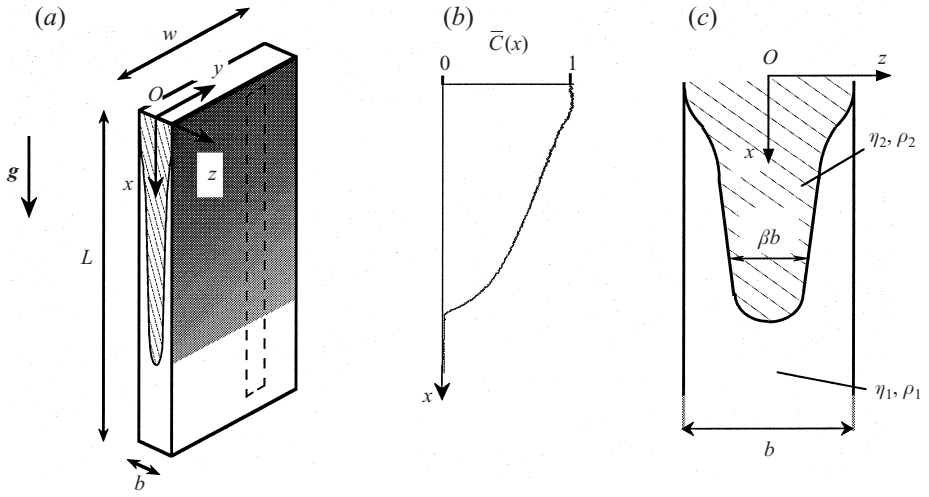


FIGURE 1. (*a*) Sketch of the two-dimensional regime mixing zone between two miscible fluids in a Hele-Shaw cell. (*b*) A typical measured concentration profile $\overline{C}(x)$. (*c*) Sketch of the interface in the gap of the Hele-Shaw cell. The relative thickness $\beta(x)$ of the tongue of fluid 2 is equal to the $z$-averaged concentration $\overline{C}(x)$.

when capillary forces across the gap are large enough (compared to viscous or buoyancy) to ensure the complete separation of the immiscible fluids: then, the meniscus spans the gap and at sufficiently small capillary numbers it has a semi-spherical shape (see also Park & Homsy 1984). At sufficiently high flow rates, however, where capillarity is small, the interface separating the two immiscible fluids does not span the gap, and may develop within the gap itself (Tabeling, Zocchi & Libchaber 1987). Then, the potential flow approach is invalid and must be re-examined. Understanding the finger shape across the gap as a function of the capillary number has been the subject of very few studies, since the classical paper by Bretherton (1961) on the motion of long bubbles in tubes, most notable being that of Park & Homsy (1984) and of Reinelt & Saffman (1985).

An analogous problem exists in the case of miscible displacement. Surprisingly, only a few experiments have addressed miscible displacements in a Hele-Shaw cell. In rectilinear displacement in a vertical cell, Wooding (1969) studied the gravitational instability between miscible fluids. Zimmerman & Homsy (1991) and Manickam & Homsy (1995) simulated numerically miscible displacements in the same geometry, assuming potential flow in the plane of the cell. The characteristics of miscible displacements in a Hele-Shaw cell at high flow rates, where viscous forces dominate, were investigated by a number of workers in recent numerical studies (Chen & Meiburg 1996; Yang 1995; Rakotomalala, Salin & Watzky 1997). These authors focused on the numerical solution of the two-dimensional problem, namely in the gap of a Hele-Shaw cell or in the axisymmetric geometry of a cylindrical tube. From the variety of techniques used, it was shown that in these geometries, miscible displacement is described by an advancing front with a well-defined interface, propagating symmetrically in the middle of the gap or of the tube (figure 1), provided that the flow velocity is large enough for diffusive effects to be negligible. The existence of a sharp interface in a tube was confirmed in experiments by Petitjeans & Maxworthy (1996). Miscible displacement experiments in a Hele-Shaw cell at high rates were conducted by Lajeunesse *et al.* (1997), where the downward displacement of a

miscible fluid by a lighter and less viscous one was studied. It was found that at sufficiently high rates, the interface between the fluids propagated as a two-dimensional symmetric tongue across the gap, as long as the velocity was below a threshold or the viscosity ratio $M$ was less than $\sim 1.5$. For $M$ larger than 1.5, there exists a velocity threshold above which this regime becomes unstable and leads to a three-dimensional fingering pattern, similar to that reported by Paterson (1985) but much different from the Saffman–Taylor finger. More recently, Snyder & Tait (1998) focused on a similar viscous instability during horizontal miscible displacement in different devices, and obtained results in qualitative agreement with Paterson (1985).

The objective of this paper is to analyse and characterize the two-dimensional regime, namely the pattern in the gap before the onset of the three-dimensional instability. Miscible displacement experiments are conducted in a Hele-Shaw cell in the presence of gravity. These are described in § 2. The displacements occur at a constant flow velocity $q$, at sufficiently high Péclet numbers ($Pe = qb/D_m \gg 1$, where $D_m$ is the molecular diffusion coefficient), so that a well-defined interface between the miscible fluids is possible. The experimental self-similar concentration profiles are analysed theoretically by extending the theory of Yang (1995) to include buoyancy effects (§ 3). The theory predicts three different kinds of interface shapes, corresponding to three different domains in the $(M, U)$-plane, where

$$M = \eta_1/\eta_2 \tag{1.1}$$

is the viscosity ratio between displaced (subscript 1) and displacing fluids (subscript 2), and $U$ is a normalized flow rate

$$U = \frac{12\eta_1 q}{b^2 \Delta\rho g} \tag{1.2}$$

expressing the ratio between viscous and buoyancy forces, where $\Delta\rho = \rho_1 - \rho_2$ is the density difference between the fluids. The boundaries between the three domains are derived in § 3, and theory and experiments are compared in § 4. For completeness, an analogous effort is also reported for the problem of miscible displacement in a cylindrical tube (§ 5).

## 2. Experimental

Miscible displacement experiments were performed in a vertical Hele-Shaw cell (figure 1), consisting of two transparent glass plates of length $L = 80\,\text{cm}$, width $W = 10\,\text{cm}$, and two different gap thicknesses $b = 0.96$ or $1.92\,\text{mm}$. The glass plates were separated by a uniform spacer, ensuring a constant gap thickness, and were thick enough to avoid bending of the plates. We used silicon oils as miscible fluids, the viscosities of which, measured with a viscometer, varied in the range 2 to 500 mPa s, while the density contrast $\Delta\rho/(\rho_1 + \rho_2)$ varied in the range 0.5% to 5%. Consequently, two decades in the viscosity ratio, $M = \eta_1/\eta_2$, were covered in these experiments. The molecular diffusivity, $D_m$, measured for each pair of fluids using the deviation of a laser beam (Sommerfeld 1954), ranged from 5 to $12 \times 10^{-7}\,\text{cm}^2\,\text{s}^{-1}$.

To obtain an initially flat horizontal interface, the cell was first partially filled from the bottom with the heavier and more viscous fluid. Then, the second fluid was introduced at the top. A stabilizing density difference was necessary to achieve the initial condition of a flat interface. This procedure took a few minutes to complete. Due to diffusion, the initial interface extended somewhat (about 0.1 mm) in the $x$-direction (which is the direction of the gravity vector). Subsequently, the displacing

fluid was injected at a constant flow rate, sufficiently large ($Pe = qb/D_m > 10^4$) to avoid fluid mixing by diffusion and to lead to a well-defined interface between the fluids. To ascertain that the fluids did not mix, we monitored the motion of the interface after abruptly terminating the injection. It was found that under the action of gravity, the interface flattened and returned to an almost sharp shape. In this high Péclet number regime, therefore, the notion of an interface is relevant. On the other hand, important diffusive mixing (visible on our concentration profiles) did occur for lower flow rates (e.g. $Pe < 10^3$), in which case the analysis to follow does not apply. The movement of the interface was visualized using a blue dye (organol blue), added to the injected fluid. This dye is appropriate for tracking the interface as its diffusion coefficient in silicon oils is close to the diffusion coefficients of the oils.

In the experiments, the main quantity of interest is the transverse average concentration profile, $\overline{C}(x, y, t) = \int_0^b C(x, y, z, t)\,\mathrm{d}z/b$, where $z$ is the coordinate in the gap and $y$ is the coordinate along the lateral dimension, which was determined as follows. A uniform incident white light, perpendicular to the cell was emitted by a light source behind the cell. The image received in front of the cell was recorded with a CCD camera, connected to a computer. The received intensity, $I(x, y)$, is related to the dye concentration, therefore to the injected fluid concentration, through the Beer–Lambert law

$$I(x, y) = I_0(x, y)\mathrm{e}^{-\alpha b\overline{C}(x,y)} \tag{2.1}$$

where $I_0$ is the initial intensity and $\alpha$ is the attenuation coefficient. Because the video device digitizes the intensity in 256 grey levels, $N_g$, however, expression (2.1) must be rewritten in terms of grey levels,

$$N_g(x, y) = N_\infty + (N_0(x, y) - N_\infty)\mathrm{e}^{-\alpha b\overline{C}(x,y)} \tag{2.2}$$

where $N_0(x, y)$ is the grey level for the cell filled with the initial fluid, measured for each experiment. $\alpha$ is a constant specific to the coloured fluid and $N_\infty$ is the grey level for the cell filled with an opaque fluid. These two numbers are estimated by a least-squares fit to data obtained from fixed concentration mixtures of the two fluids, as illustrated in figure 2, where the measured data are reported along with estimated error bars. Under conditions of a two-dimensional regime, where the flow does not vary along the $y$-direction, we have the ability to average over a relatively large rectangular window, which results in a considerable reduction of the noise. In these experiments, the overall accuracy of the concentration measurement was estimated to be of the order of $4 \times 10^{-2}$ to $8 \times 10^{-2}$, while the spatial resolution varied in the range 20 to 40 pixel per cm.

A snapshot of a typical transversely averaged concentration profile $\overline{C}(x, y, t)$ is shown in figure 1, along with a sketch of the experiment. In this particular experiment, the transversely averaged concentration is independent of the lateral coordinate $y$, and in the remainder we will denote it simply as $\overline{C}(x, t)$. These data were analysed as follows. The concentration profile $\overline{C}(x, t)$ is measured at regular time intervals $\Delta t$ (figure 3*a*). From this set of data, the velocity of propagation of each concentration can be extracted, by recording the location $x$ versus time $t$ of each concentration level (50 levels corresponding to increments of 0.02 were selected). The resulting curves (figure 3*b*) were found to be linear, indicating that any given concentration $\overline{C}$ travels at a constant velocity, $V(\overline{C}) = (\partial x/\partial t)_{\overline{C}}$, which is the slope of the corresponding straight line. This behaviour is suggestive of a kinematic wave and is to be described in detail below. The values for $\overline{C}(x, t)$ and $V(\overline{C})$ so obtained were next compared to the theoretical predictions. In particular, $\overline{C}$ vs. $V$ diagrams were constructed.

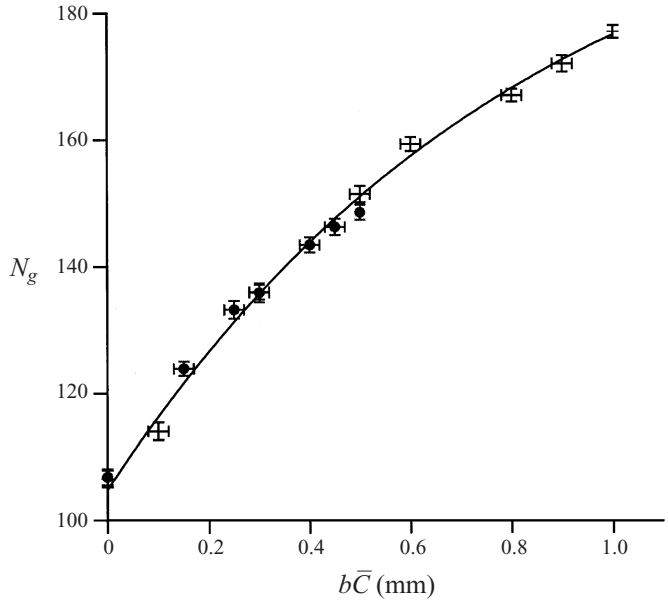


FIGURE 2. The light intensity $N_g$ received by the camera vs. $b\overline{C}$ for two values of the gap $b$ of the cell: $b = 1.92$ mm (crosses), 0.96 mm (circles). The solid line is a least-squares fit to the data, using equation (2.2).

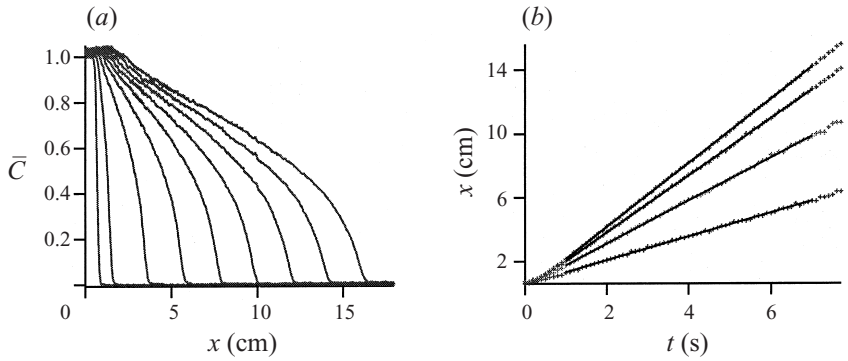


FIGURE 3. Experimental measurement of the concentration velocity $V(\overline{C})$. (*a*) Typical concentration profiles at regular time intervals. (*b*) The location $x$ of a given concentration $\overline{C}$, plotted vs. time, gives a straight line, the slope of which is $V(\overline{C})$. The straight lines shown correspond to $\overline{C} = 0.2$, 0.4, 0.6 and 0.8.

Under the conditions of a two-dimensional regime, two types of concentration profiles were observed. For values of $M$ lower than a threshold $M_T$, where $M_T \sim 1.5$, and high enough values of the normalized flow rate $U$, self-spreading profiles were obtained (figure 4*a*). We will denote these as corresponding to case 1. A decrease in $U$ resulted in profiles involving an internal shock across two concentration values $\overline{C}_m$ and $\overline{C}_M$ ($0 < \overline{C}_m < \overline{C}_M$). This shock was preceded by an advancing, self-spreading foot ($0 < \overline{C} < \overline{C}_m$), the tip of which moved at a constant ($q$-normalized) velocity $V(0) = 1.5$, while the shock itself travelled at a velocity $V_S < 1.5$ (figure 4*b*). We will denote these profiles as belonging to case 2. Such an advancing foot was also

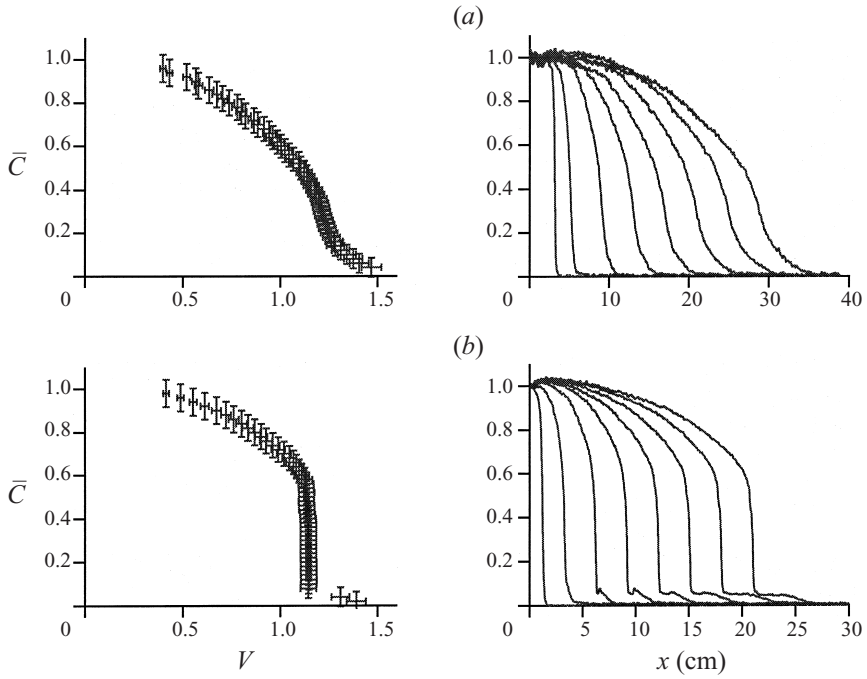


FIGURE 4. Experimental velocity profiles (left) and concentration profiles at regular time intervals (right), for $M = 0.22 < M_T \sim 1.5$, and (*a*) $U = 0.53$, (*b*) $U = 0.21$. The decrease of the flow rate allows the passage from case 1 (self-spreading, (*a*)) to case 2 (shock between $\overline{C}_m > 0$ and $\overline{C}_M$, with a velocity $V_S < 1.5$, (*b*)).

observed experimentally by Petitjeans & Maxworthy (1996) and numerically by Chen & Meiburg (1996).

For $M > M_T$ profiles pertaining to case 2 were still observed, provided that the velocities were sufficiently low. When the flow rates exceeded an $M$-dependent threshold value $U_T(M)$, a three-dimensional instability appeared (case 3). In this case, the concentration pattern exhibited a three-dimensional structure, consisting of a series of three-dimensional fingers regularly spaced in the $y$-direction and separated by a tiny slice of initial fluid, as already reported in Lajeunesse *et al.* (1997). The observed width of the fingers is close to that measured for non-buoyant miscible displacements in a Hele-Shaw cell, by Paterson (1985) in a radial geometry ($\sim 4b$), and by Snyder & Tait (1998) in a rectilinear flow geometry ($\sim 2b$). It is also compatible with the radius of curvature ($\sim 2.5b$) of the anomalous Saffman–Taylor fingers measured by Rabaud, Couder & Gérard (1988) in their immiscible displacement experiments, in the limit of high capillary numbers.

Figure 5 illustrates the evolution of the profiles of case 2, for $M > M_T$, as a function of $U$: as $U$ increases, the extent of the foot decreases, while the shock velocity increases. At a velocity, to be denoted by $U_{23}(M)$, the internal shock velocity becomes 1.5 and the preceding foot disappears (to within experimental accuracy), and the internal shock now becomes a frontal shock. Following a further increase in $U$, there is a transition region, to be discussed below, where the flow regime is still two-dimensional, and contains a frontal shock of velocity approximately equal to 1.5. As discussed above, at a critical velocity $U_T > U_{23}$, the two-dimensional regime destabilizes to the three-dimensional regime (case 3). Thus, we find experimentally

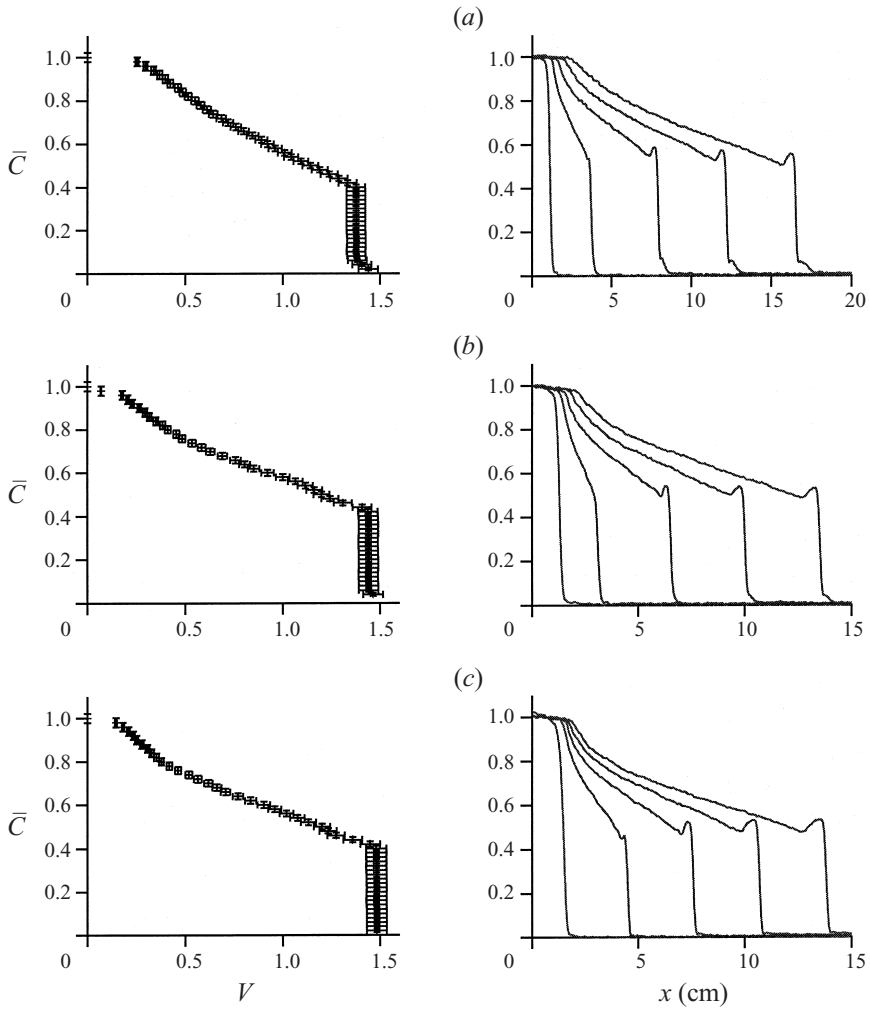


FIGURE 5. Experimental velocity profiles (left) and concentration profiles at regular time intervals (right), for $M = 10.5 > M_T$, and (*a*) $U = 0.58$, (*b*) $U = 0.70$, and (*c*) $U = 1.20 < U_T = 1.62$. As $U$ is increased and approaches the three-dimensional instability threshold $U_T$, the shock velocity increases, whereas the extent of the preceding foot decreases.

that the onset of the transition towards the three-dimensional instability possibly corresponds, in the two-dimensional regime, to conditions such that the shock velocity exceeds 1.5, after the disappearance of the preceding foot. A theoretical analysis of the two-dimensional profiles is proposed in the following section.

## 3. Theory

To analyse the two-dimensional regime (cases 1 and 2), in which the self-similar experimental profiles have features of kinematic waves, we will make use of the approach of Yang & Yortsos (1997) (see also Yang 1995). These authors addressed the problem of describing the two-dimensional shape of the interface between two miscible Newtonian fluids flowing between two parallel plates or in a cylindrical tube, in the absence of buoyancy and at large values of the Péclet number $Pe$. They

proposed an asymptotic method in the combined limits of infinitely large $Pe$ and infinitely long plates (or infinitely long tube), compared to the spacing between the plates (or the tube radius). In this section, we summarize their approach and extend their model to the case of the Hele-Shaw cell, by taking into account buoyancy effects. For reasons related to the experimental procedure (see previous section), we will restrict our analysis to the gravity stabilized case (where a lighter fluid is injected from the top).

### 3.1. *Formulation*

Consider the downward miscible displacement along the vertical $x$-axis of a Hele-Shaw cell, of fluid 1 by fluid 2, at a constant injection rate $q$. We assume that the invading fluid forms a symmetric tongue across the gap, invariant along the width $W$ and characterized by its relative thickness $\beta(x,t)$, which here is equal to $\overline{C}(x,t)$ (figure 1). We are interested in calculating the long time evolution of the shape of this tongue.

We proceed by writing a mass balance for fluid 2, averaged across the gap $b$ (along the $z$-axis). Then,

$$\frac{\partial \overline{C}(x,t)}{\partial t} + \frac{\partial qF(x,t)}{\partial x} = 0 \tag{3.1}$$

where $\overline{C}(x,t)$ and $F(x,t)$ are the transverse average of the local concentration $C(x,z,t)$, and the $q$-normalized flux function of fluid 2, respectively, namely

$$\overline{C}(x,t) = \frac{1}{b}\int_{-b/2}^{+b/2} C(x,z,t)\,\mathrm{d}z, \tag{3.2}$$

$$F(x,t) = \frac{1}{qb}\int_{-b/2}^{+b/2} C(x,z,t)u(x,z,t)\,\mathrm{d}z, \tag{3.3}$$

where $u$ is the velocity component in the $x$-direction. As in Yang & Yortsos (1997) we make the following hypotheses.

(H1): $Pe = qb/D_m \gg 1$. The injection rate $q$ is sufficiently large to prevent diffusive mixing of the fluids. It follows that $C(x,z,t) = 0$ for $|z| > \frac{1}{2}b\beta(x,t)$ and $C(x,z,t) = 1$ for $|z| < \frac{1}{2}b\beta(x,t)$.

(H2): $\partial b\beta/\partial x \ll 1$. The tongue is developed over a length $l \gg b$, leading to a quasi-parallel flow condition ($v \ll u$, where $v$ is the transverse velocity component) (figure 6).

(H3): $qb^2/\nu l \ll 1$. The fluids are sufficiently viscous so that the unsteady term in the Stokes equation can be neglected (quasi-stationary flow).

Under the above hypotheses, a kinematic wave theory, in which the flux function $F$ is expressed in terms of $\overline{C}$, can be developed. For this, we first note that in view of (H1), equations (3.2) and (3.3) become

$$\overline{C}(x,t) = \beta(x,t), \tag{3.4}$$

$$F(x,t) = \frac{2}{qb}\int_{0}^{+b\beta/2} u(x,z,t)\,\mathrm{d}z. \tag{3.5}$$

The velocity component $u$ obeys the Stokes equation

$$0 = -\frac{\mathrm{d}P}{\mathrm{d}x} + \eta_i\frac{\mathrm{d}^2u}{\mathrm{d}z^2} + \rho_i g \tag{3.6}$$

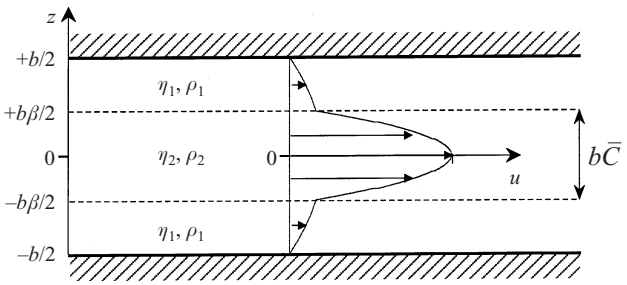


FIGURE 6. The fluid configuration in the gap of the cell under the quasi-parallel flow hypothesis, and the corresponding parabolic velocity profile in each fluid.

where $i = 2$ for $|z| < \frac{1}{2}b\beta$ and $i = 1$ otherwise. The resulting velocity profile is a parabola within each fluid (figure 6), and satisfies no-slip boundary conditions at the solid walls (fluid 1), and velocity and viscous stress continuity at the fluid interface $z = \pm b\beta/2$. Given that the local pressure gradient $\mathrm{d}P/\mathrm{d}x$ is the same for both fluids, it can be eliminated by using the condition of a constant injection rate. Thus, $u$ depends only on the variables $z$ and $\overline{C}$, and can be obtained in a straightforward fashion. Substituting the expression so obtained for $u$ in (3.5) leads to the flux function $F$ in terms of $\overline{C}$ only. After several calculations, one obtains

$$F(\overline{C}) = \frac{\overline{C}}{2}\frac{[(2M-3)\overline{C}^2+3]}{[1+(M-1)\overline{C}^3]} + \frac{\overline{C}^2(1-\overline{C}^3)}{4U}\frac{[(4M-3)\overline{C}+3]}{[1+(M-1)\overline{C}^3]} \tag{3.7}$$

where the viscosity ratio $M$ and the normalized flow rate $U$ (defined in (1.1) and (1.2)) are the control parameters. Then, the conservation equation (3.1) takes the form of a quasi-linear hyperbolic equation

$$\frac{\partial \overline{C}(x,t)}{\partial t} + q\frac{\partial F(\overline{C}(x,t))}{\partial x} = 0 \tag{3.8}$$

which can be analysed using kinematic wave theory (Whitham 1974; Jeffrey 1976; Yang & Yortsos 1997).

### 3.2. *Kinematic wave theory*

The hyperbolic equation (3.8) has the well-known property that the normalized velocity of each concentration $\overline{C}$ (each point of the interface $(x, \beta(x,t))$ in our case) is only $\overline{C}$-dependent

$$V(\overline{C}) \equiv \frac{1}{q}\left(\frac{\partial x}{\partial t}\right)_{\overline{C}} = \frac{\mathrm{d}F}{\mathrm{d}\overline{C}}. \tag{3.9}$$

This relation holds under the assumption that $\overline{C}(x,t)$ is differentiable. The time evolution of a general differentiable profile, $\overline{C}(x,t)$, depends on the shape of $F(\overline{C})$ (figure 7). For a monotonically varying profile, which is the case of interest to this paper, two possibilities exist.

(i) $\mathrm{d}^2F/\mathrm{d}\overline{C}^2 \leqslant 0$ for $0 \leqslant \overline{C} \leqslant 1$.

Here, $V(\overline{C})$ is a monotonically decreasing function, such that the smaller the concentration, the larger its velocity. The leading part of the interface travels faster than the trailing, yielding a continuous, self-spreading concentration profile (figure 7*a*).

(ii) $\mathrm{d}^2F/\mathrm{d}\overline{C}^2 \geqslant 0$ for $\overline{C}_1 \leqslant \overline{C} \leqslant \overline{C}_2$ and $\mathrm{d}^2F/\mathrm{d}\overline{C}^2 \leqslant 0$ otherwise.

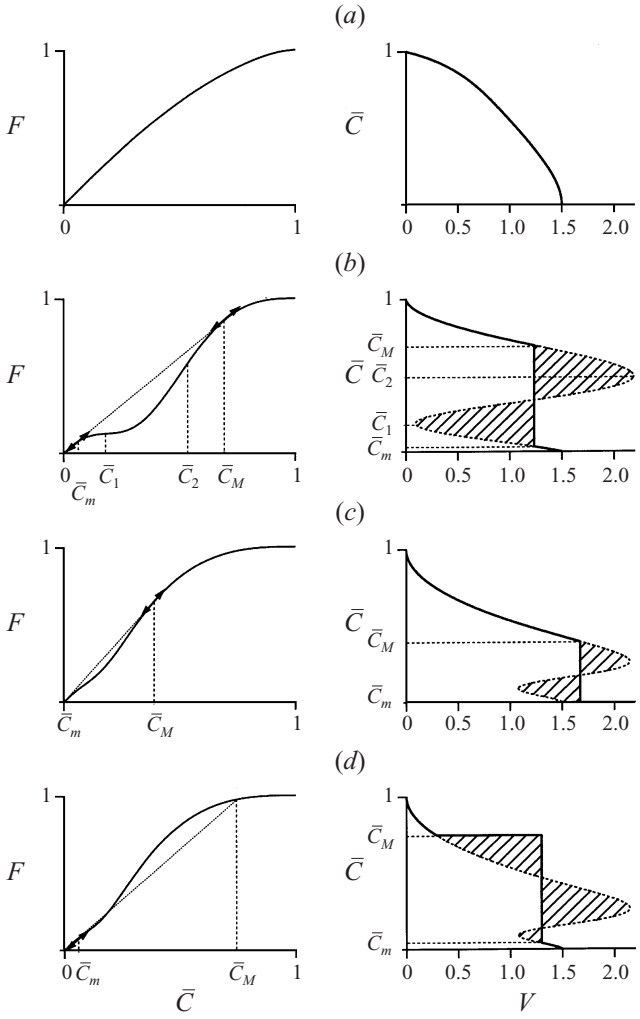


FIGURE 7. Left: flux function $F(\overline{C})$: the slope of the dotted straight line between $\overline{C}_m$ and $\overline{C}_M$ gives the shock velocity $V_S$; the arrows indicate the points at which this line is tangent to the curve. Right: $\overline{C}$ vs. the concentration velocity $V$ (full line) and $\mathrm{d}F/\mathrm{d}\overline{C}$ (dotted line). (*a*) $\mathrm{d}^2F/\mathrm{d}\overline{C}^2 \leqslant 0$ in the whole concentration range. Then, $V = \mathrm{d}F/\mathrm{d}\overline{C}$ decreases monotonically with $\overline{C}$ (domain 1). (*b*) $\mathrm{d}^2F/\mathrm{d}\overline{C}^2 \geqslant 0$ in the range $[\overline{C}_1, \overline{C}_2]$. Geometric construction of a contact shock with a velocity $V_S$, between $\overline{C}_m$ and $\overline{C}_M$, ensuring that $V(\overline{C})$ is a decreasing continuous function of $\overline{C}$ and satisfying the overall mass conservation of fluid 2 (domain 2). (*c*) $\mathrm{d}^2F/\mathrm{d}\overline{C}^2 \geqslant 0$ in the range $[\overline{C}_1, \overline{C}_2]$. Geometric construction of a contact shock between 0 and $\overline{C}_M$ with a velocity $V_S > 1.5$, (domain 3). (*d*) Same flux curve as for (*c*). Geometric construction of a possible shock with a velocity $V_S < 1.5$, between $\overline{C}_m > 0$ and $\overline{C}_M$, in the absence of continuity for $V(\overline{C})$.

Here, on the other hand, $V(\overline{C})$ increases between $\overline{C}_1$ and $\overline{C}_2$. In this range, larger concentrations travel faster than smaller ones, eventually passing them. This would lead to an unphysical triple-valued solution for $\overline{C}$, unless equation (3.9) loses its validity in the range $[\overline{C}_1, \overline{C}_2]$, and $\overline{C}(x,t)$ ceases to be differentiable. Then, the multi-valued solution must be replaced by an (internal) shock (a concentration step, figure 7*b*) between two concentrations $\overline{C}_m$ and $\overline{C}_M$ such that

$$\overline{C}_m \leqslant \overline{C}_1 \quad \text{and} \quad \overline{C}_M \geqslant \overline{C}_2. \tag{3.10}$$

As the profile is no longer differentiable in this region, the velocity of the shock is given by the global relation of conservation of fluid 2 across the shock region:

$$V_S(\overline{C}_m, \overline{C}_M) = \frac{F(\overline{C}_m) - F(\overline{C}_M)}{\overline{C}_m - \overline{C}_M}. \tag{3.11}$$

In this case, $V(\overline{C})$ is equal to $\mathrm{d}F/\mathrm{d}\overline{C}$ for $\overline{C} \leqslant \overline{C}_m$ and $\overline{C} \geqslant \overline{C}_M$, and to the constant value $V_S$ for $\overline{C}_m \leqslant \overline{C} \leqslant \overline{C}_M$. Furthermore, $V(\overline{C})$ has to be a decreasing function of $\overline{C}$ to cope with the unphysical situation mentioned above, which reads

$$\frac{\mathrm{d}F}{\mathrm{d}\overline{C}}(\overline{C}_M) \leqslant \frac{F(\overline{C}_m) - F(\overline{C}_M)}{\overline{C}_m - \overline{C}_M} \leqslant \frac{\mathrm{d}F}{\mathrm{d}\overline{C}}(\overline{C}_m). \tag{3.12}$$

The shock-delineating concentrations $\overline{C}_m$ and $\overline{C}_M$ can be calculated if one assumes that $V(\overline{C})$ is continuous (contact internal shock). In this case, $\overline{C}_m$ and $\overline{C}_M$ are given by the relations

$$\frac{F(\overline{C}_m) - F(\overline{C}_M)}{\overline{C}_m - \overline{C}_M} = \frac{\mathrm{d}F}{\mathrm{d}\overline{C}}(\overline{C}_m) = \frac{\mathrm{d}F}{\mathrm{d}\overline{C}}(\overline{C}_M). \tag{3.13}$$

The geometric construction for the determination of $\overline{C}_m$, $\overline{C}_M$ and $V_S(\overline{C}_m, \overline{C}_M)$ from the flux curve is sketched on the left of figure 7(*b*): the dotted straight line joining the points corresponding to $\overline{C}_m$ and $\overline{C}_M$ on the flux curve has a slope equal to the shock velocity $V_S$. Then, equation (3.13) is satisfied when this line is tangent to the curve at both $\overline{C}_m$ and $\overline{C}_M$. On the right of figure 7(*b*), $V(\overline{C})$ is equal to $\mathrm{d}F/\mathrm{d}\overline{C}$ below $\overline{C}_m$ and above $\overline{C}_M$ (equation (3.9)), while in-between (shock) the shock velocity $V(\overline{C}) = V_S$ is such that the shaded areas enclosed by the dotted lines are equal (equation (3.11)).

In the particular case where no solutions ($\overline{C}_m$, $\overline{C}_M$) of (3.13) can be found in the range [0, 1], the contact shock is given by (0, $\overline{C}_M$) (or ($\overline{C}_m$, 1)), which solve part of equation (3.13), namely without the term $(\mathrm{d}F/\mathrm{d}\overline{C})(\overline{C}_m)$ (or $(\mathrm{d}F/\mathrm{d}\overline{C})(\overline{C}_M)$). The shock velocity is then greater than $(\mathrm{d}F/\mathrm{d}\overline{C})(0)$ (or smaller than $(\mathrm{d}F/\mathrm{d}\overline{C})(1)$), as illustrated in figure 7(*c*); in this case, the dotted straight line is not tangent to the flux curve at $\overline{C}_m = 0$ (or $\overline{C}_M = 1$). We must also mention that the contact shock is not the only acceptable solution, as $V(\overline{C})$ does not need to be continuous: any shock with a velocity given by (3.11) and fulfilling the conditions (3.10) and (3.12) can be a physical solution. An example of the geometric construction of such a solution is given in figure 7(*d*), for the same flux curve as in figure 7(*c*). In the particular case when the shock is not of the contact type and has a concentration at the leading edge equal to zero, we will denote this as a frontal shock.

Consider, now, the application to our problem. An analysis of the properties of the flux function given by equation (3.7) shows that three different domains can be defined in the $(M, U)$-plane, corresponding to three possible types of profiles.

Domain 1: no shock occurs and the entire profile is self-spreading (figure 7*a*). Here, the velocity of the leading edge, $V(0) = (\mathrm{d}F/\mathrm{d}\overline{C})(0)$, is equal to $V_0 = 1.5$.

Domain 2: the profile includes a contact internal shock travelling at a velocity $V_S < V_0$ along with a foot preceding the shock (figure 7*b*). Here, the shock occurs in the range $[\overline{C}_m, \overline{C}_M]$, with $\overline{C}_m > 0$, outside which the profile is self-spreading. The velocity of the leading edge of the foot advancing ahead of the shock is $V_0$.

Domain 3: the profile includes a shock travelling at a velocity $V_S \geqslant V_0$ (figure 7*c*). Now, $\overline{C}_m = 0$ (there is no leading foot), and the profile is self-spreading for $\overline{C} > \overline{C}_M$. Here, we need to make a further distinction: frontal shocks of the contact type are predicted by the theory to travel in this region with a velocity $V_S > V_0$; however,

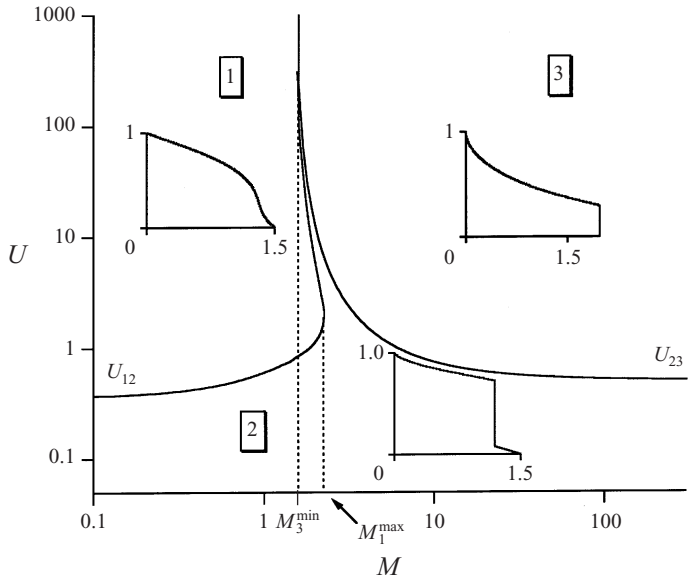


FIGURE 8. The boundaries $U_{12}(M)$ and $U_{23}(M)$, derived from equation (3.7), delineate in the $(M, U)$-plane the domains 1, 2 and 3. $M_1^{\max} = 2.25$ and $M_3^{\min} = 1.5$ are the upper limit for domain 1 and the lower limit for domain 3, respectively.

other shocks (not of the contact type) are also possible, provided that they satisfy shock condition (3.11). In the case where $\overline{C}_m = 0$, these would be frontal shocks. In either case, their velocity is less than that of the corresponding contact shock. Such frontal shocks were identified in the two-dimensional numerical experiments of Chen & Meiburg (1996) and Rakotomalala *et al.* (1997) and were discussed in Yang & Yortsos (1997). They also appear in our experiments in this region, see below.

Note that, whatever the values of $M$ and $U$, $(\mathrm{d}F/\mathrm{d}\overline{C})(0)$ remains equal to $V_0 = 1.5$, which represents the maximum Poiseuille velocity in single-phase flow between two parallel plates.

The three domains are depicted in the $(M, U)$-plane of figure 8. The boundary, $U = U_{23}(M)$, between domains 2 and 3, is determined by requiring that the self-spreading foot at the front of the concentration profile disappears (at which point the contact-shock velocity is equal to $V_0$) . This boundary has a surprisingly simple analytical form

$$U_{23} = \frac{8M^3}{(2M-3)^2(4M-3)} \quad \text{and } M > M_3^{\min}, \tag{3.14}$$

with

$$M_3^{\min} = 1.5. \tag{3.15}$$

The value $\overline{C}_{23}$ of $\overline{C}_M$ at this transition is

$$\overline{C}_{23} = \frac{2M-3}{4M-3}. \tag{3.16}$$

The boundary, $U = U_{12}(M)$, between domains 1 and 2 is determined by requiring a single inflection point on the flux curve (at which point the $\overline{C}(V)$ profile for the first time acquires a divergent derivative). One can show numerically that the necessary condition for the existence of domain 1 is $M \leqslant M_1^{\max}$ with $M_1^{\max} = 2.25$. We note that

the boundary $U_{12}(M)$ has the same asymptotic limit at large $U$ as $U_{23}(M)$, which is $M = M_3^{\min} = 1.5$. Thus, our analysis recovers the non-buoyant case ($U \to \infty$) studied by Yang & Yortsos (1997), where domain 2 does not exist. Note also that for $M$ values in the interval $[M_3^{\min}, M_1^{\max}]$, the curve $U_{12}(M)$ is double-valued. Thus, for a given value of $M$ in this range, a continuous increase of the flow rate $U$ allows one to successively explore domain 2, then domain 1, and then domain 2 again, before the transition to domain 3 at $U = U_{23}(M)$.

In the following section, the kinematic wave theory will be compared to experimental results. Before we proceed, however, the following remarks are appropriate.

### 3.3. *Remarks*

Under the conditions of domain 1, the assumption of a local quasi-parallel flow (H2) is being satisfied increasingly better as time elapses. On the other hand, the same assumption will lose validity in the vicinity of the sharp front (shock) under conditions for the validity of domains 2 and 3. In this region, the continuity of the fluid velocity across the shock requires a transition zone of finite length $l_S$ ($l_S > 0$), where both velocity components must be kept. The length $l_S$ has to be of the order of $b$, and must remain constant as the shock propagates (stationary travelling front). Indeed, if $l_S$ happened to be much larger than $b$, hypothesis (H2) would again be fulfilled, leading to a subsequent sharpening of this zone, according to the above. The velocity field in the transition zone should be governed by the full Stokes equations in two dimensions, and approach asymptotically the uni-directional, parallel velocity fields, upstream and downstream of the front. In general, therefore, the values of $\overline{C}_m$ and $\overline{C}_M$ satisfying the above conditions may differ from those corresponding to a contact shock (see also Yang & Yortsos 1997), yielding a non-continuous $V(\overline{C})$. Moreover, as no prediction is given for the concentration profile in the transition zone across the shock, the profile does not necessarily vary monotonically in this region (e.g. this may be the origin of the features on the right of figure 5). What is necessary, from the study of the flux curve, is that, whatever the actual values of $\overline{C}_m$ and $\overline{C}_M$, the shock velocity cannot be greater than $V_0 = 1.5$ in domain 2. What is not necessary, is the existence of a leading foot in domain 2, and the condition $V_S > V_0$ in the experimental profiles pertaining to domain 3.

In summary, the kinematic wave approach rigorously predicts the long-time evolution of self-spreading profiles, delineates the domain where these profiles can occur (boundary $U_{12}(M)$), and provides the flow rate below which the shock velocity cannot be greater than $V_0$ (boundary $U_{23}(M)$).

## 4. Comparison between theory and experiments

Typical experimental profiles are compared to the theoretical ones in figure 9. As expected, the self-spreading profiles (case 1, figure 9*a*) are well reproduced by the theory. The agreement still holds for the two-dimensional profiles with an internal contact shock (case 2), obtained either at $M < M_1^{\max}$ (figure 9*b*) or $M > M_1^{\max}$ (figure 9*c*). In fact, all the experiments pertaining to cases 1 and 2 were found to compare well both qualitatively and quantitatively, with the corresponding profiles in the domains 1 and 2.

Figure 10 shows theoretical and experimental results for the shock velocity and the shock limiting concentrations for $M = 10.5 > M_3^{\min}$, where the experiments probe domains 2 and 3. Also reported in the figure are the theoretical threshold for a frontal shock, $U_{23}$, and the experimental threshold for instability, $U_T$, respectively.

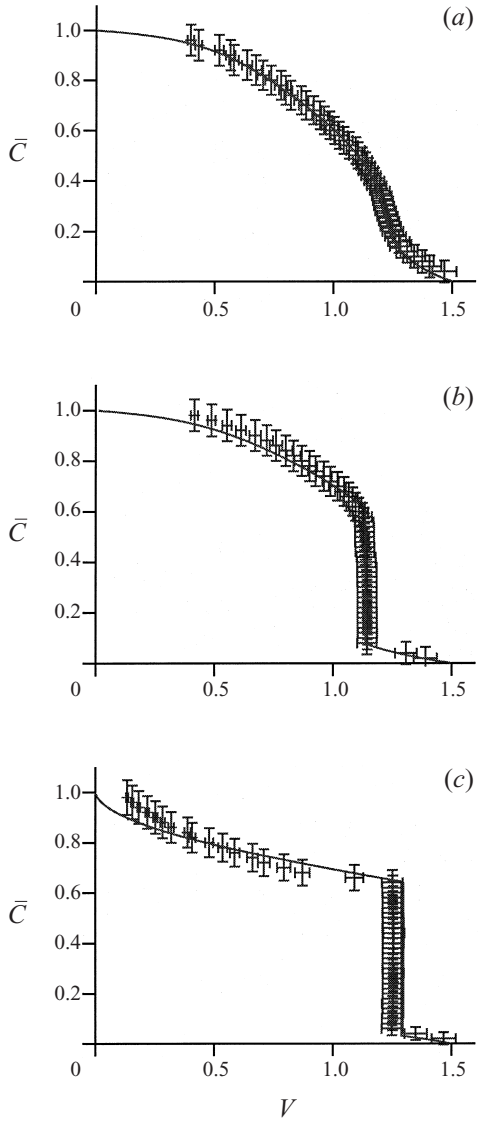


FIGURE 9. Comparison between experimental (symbols) and theoretical (solid lines) velocity profiles for (*a*) $M = 0.22$, $U = 0.53 > U_{12} = 0.39$, (*b*) $U = 0.21 < U_{12}$, and (*c*) $M = 12.2$ and $U = 0.31 < U_{23} = 0.69$.

The agreement between experiments and theory is quite satisfactory for $U < U_{23}$. In particular, the existence of an internal contact shock between the two limiting concentrations $0 < \overline{C}_m < \overline{C}_M$ is well recovered in the experiments. In addition, the self-spreading foot at the leading edge of the interface was found to move with the expected velocity $V(0) = V_0 = 1.5$. For $U > U_{23}$, a deviation of the experimental values of $V_S$, $\overline{C}_M$ and $\overline{C}_m$ from the theoretical ones, obtained under the assumption of a *contact* shock is observed, however. The measured values of $V_S$ remain close to 1.5, the corresponding $\overline{C}_M$ are larger than the calculated ones, whereas $\overline{C}_m$ values greater than zero are still observed. In other words, case 2 profiles were obtained in the calculated domain 3. This discrepancy supports the contention that such shocks

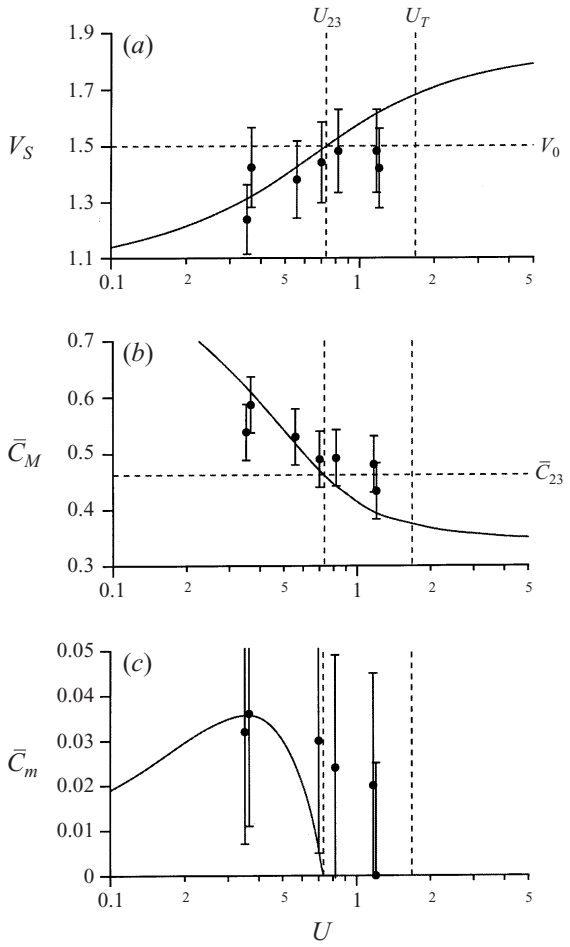


FIGURE 10. Comparison between experimental (dots) and theoretical predictions (solid lines) for the variations of (*a*) $V_S$, (*b*) $\overline{C}_M$ and (*c*) $\overline{C}_m$, vs. $U$, for $M = 10.5$. The dashed vertical lines indicate the theoretical $U_{23} = 0.73$ and experimental $U_T = 1.62$, the dashed horizontal lines indicate the calculated $V_0 = 1.5$ and $\overline{C}_{23} = 0.46$.

are not any more of the contact type (figure 7*d*). These features were common to all experiments performed at $M > M_T$: the experimental profiles obtained at $U \leqslant U_{23}$ were satisfactorily described by the theory (domain 2), whereas a two-dimensional regime not involving contact shocks (with $V_S \simeq 1.5$) was observed in a limited range of flow rates, $U_{23} < U < U_T$, above which the three-dimensional instability occurred. Hence, $U_{23}(M)$ must be interpreted as serving as a lower bound to the transition observed at $U = U_T$.

The main findings of this work are displayed in the $(M, U)$-plane of figure 11, where the symbols denote experiments, while the solid lines are theoretical boundaries. Filled symbols represent the experimental results which were quantitatively described by the theory. In particular, the experiments at $M = 2$ (where $M_3^{\min} < M < M_1^{\max}$) explored successively domains 2, 1 and 2 again, for increasing flow rates, as predicted from the theory. Figure 11 shows that the kinematic wave theory provides a quantitative description for the entire field $M < M_3^{\min}$ or $U < U_{23}$, under the assumptions of low Reynolds and high Péclet numbers (which define, for each pair of fluids, a range of

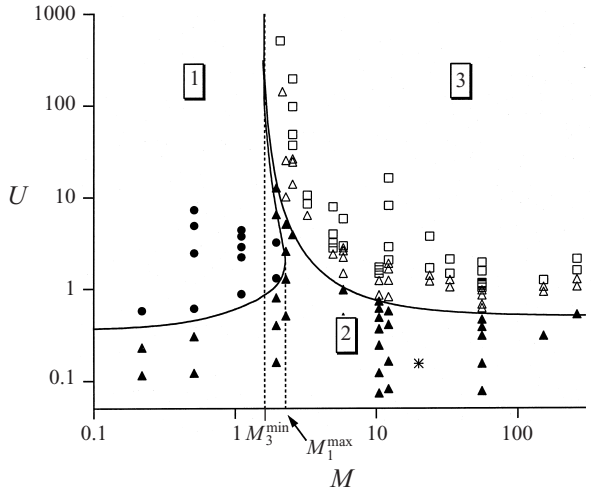


FIGURE 11. Classification, in the $(M, U)$-plane, of the main results obtained in the Hele-Shaw cell. Filled symbols indicate experiments described quantitatively by the theory (circles: self-spreading profiles, triangles: profiles with a shock travelling at $V_S < 1.5$). Open triangles show the cases of disagreement between measured two-dimensional profiles and theory, and open squares correspond to the observation of three-dimensional patterns. The lines are the theoretical boundaries $U_{12}(M)$ and $U_{23}(M)$ delineating domains 1, 2 and 3, and the star corresponds to the simulation by Chen & Meiburg (1996).

validity for $U$, that increases with $vL/D_m b$). The parameters used by Chen & Meiburg (1996) to simulate their 'unsteady' regime (similar to our case 2 profiles), fall in domain 2 (star in figure 11). Open squares represent experiments where the three-dimensional patterns were observed, invalidating the kinematic wave description. Below these points and above $U_{23}$, the zone containing open triangles corresponds to the range of flow rates where the two-dimensional measured profiles disagree with the theoretical predictions based on a contact shock. Although the curve $U_{23}(M)$ is only a lower bound to the experimental curve $U_T$, our on-going investigation suggests that the $M$-threshold for the onset of the instability, $M_T$, does correspond to the theoretical value $M_3^{\min} = 1.5$. We also mention that the experimental values $U_T(M)$ may actually constitute an upper bound to the true threshold, given that the cell has a finite length ($L = 80\,\text{cm}$), and that it is possible that instabilities could take a time longer than $\sim L/q$ to develop for flow rates in the range $[U_{23}, U_T]$.

## 5. Displacement in a vertical tube

An analogous experimental and theoretical effort was made to study miscible displacement at high rates in a long vertical tube. The previous kinematic approach was used to analyse this displacement as well. Consider the downward vertical miscible displacement of fluid 1 by a fluid 2 at a constant injection rate $q$ in a cylindrical tube of radius $R$, with its axis oriented along the vertical $x$-direction. Owing to the symmetry of the problem, the invading fluid forms an axisymmetric finger described by its relative radius $\beta(x, t)$. The flow can then be treated by the same two-dimensional approach and under the same hypotheses as in the previous case of parallel plates. Now, the average concentration $\overline{C}(x, t)$ is related to $\beta(x, t)$ through

$$\overline{C}(x, t) = \beta^2(x, t) \tag{5.1}$$

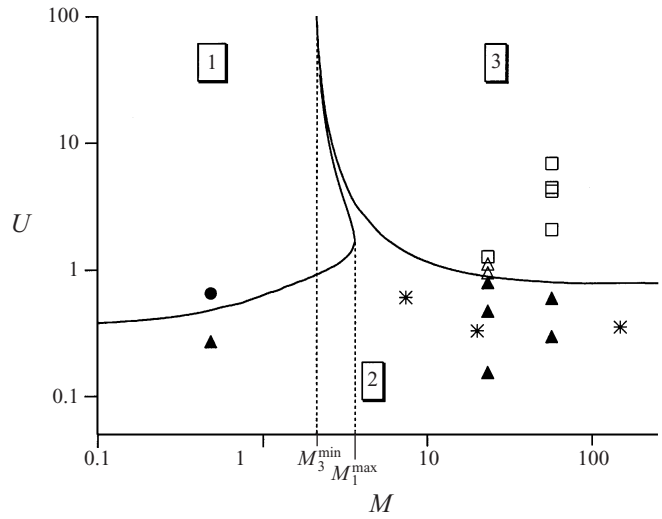


FIGURE 12. Calculated domains 1, 2 and 3 for displacement in a tube. $M_1^{\max} = 3.6$ and $M_3^{\min} = 2$ are the upper limit for domain 1 and the lower limit for domain 3, respectively. Symbols indicate experiments found in quantitative agreement (filled) or disagreement (open) with theoretical predictions (circles: self-spreading profiles, triangles: profiles with a shock travelling at $V_S < 2$, squares: profiles with a shock travelling at $V_S > 2$). The stars correspond to the simulations by Chen & Meiburg (1996).

and the flux function $F(\overline{C})$ reads

$$F(\overline{C}) = \overline{C}\frac{(M-2)\overline{C}+2}{1+(M-1)\overline{C}^2} + \frac{\overline{C}^2}{U}\frac{(1-\overline{C})[4-M+(4+3M)\overline{C}]}{1+(M-1)\overline{C}^2} + \frac{2\overline{C}^2}{U}\ln\overline{C}, \qquad (5.2)$$

where the normalized flow velocity $U$ is given by

$$U = \frac{8\eta_1 q}{R^2\Delta\rho g}. \qquad (5.3)$$

Application of the kinematic wave theory shows that the concentration $\overline{C} = 0$ travels at the normalized velocity $V(0) = (\mathrm{d}F/\mathrm{d}\overline{C})(0) = V_0 = 2$, which is the maximum Poiseuille velocity for fluid flow in a tube.

Working exactly as before, we find that there exist three different domains in the $(M, U)$-plane: domain 1 contains self-spreading profiles in the absence of a shock, domain 2 consists of profiles with an internal shock of the contact type, travelling at $V_S < V_0$, and self-spreading segments ahead of and behind the shock, while domain 3 corresponds to profiles with a frontal, contact shock of velocity $V_S > V_0$. The boundaries $U_{12}(M)$ and $U_{23}(M)$, separating these domains, are displayed in the $(M, U)$-plane of figure 12. This diagram is very similar to that for the Hele-Shaw problem, except that $M_3^{\min} = 2$ and $M_1^{\max} = 3.6$. Many of the features identified in the previous analysis hold here as well.

In order to test the theoretical predictions, a few miscible displacement experiments were conducted using the same procedure as described in the Hele-Shaw cell case. A vertical cylindrical tube of length of 1 m and radius $R = 6$ mm, made of PMMA, was used. Figure 13 shows snapshots of the displacement at different times for a particular experiment corresponding to domain 2. For quantitative purposes, the cross-sectionally averaged concentration, $\overline{C}(x, t)$, was measured using an analogous

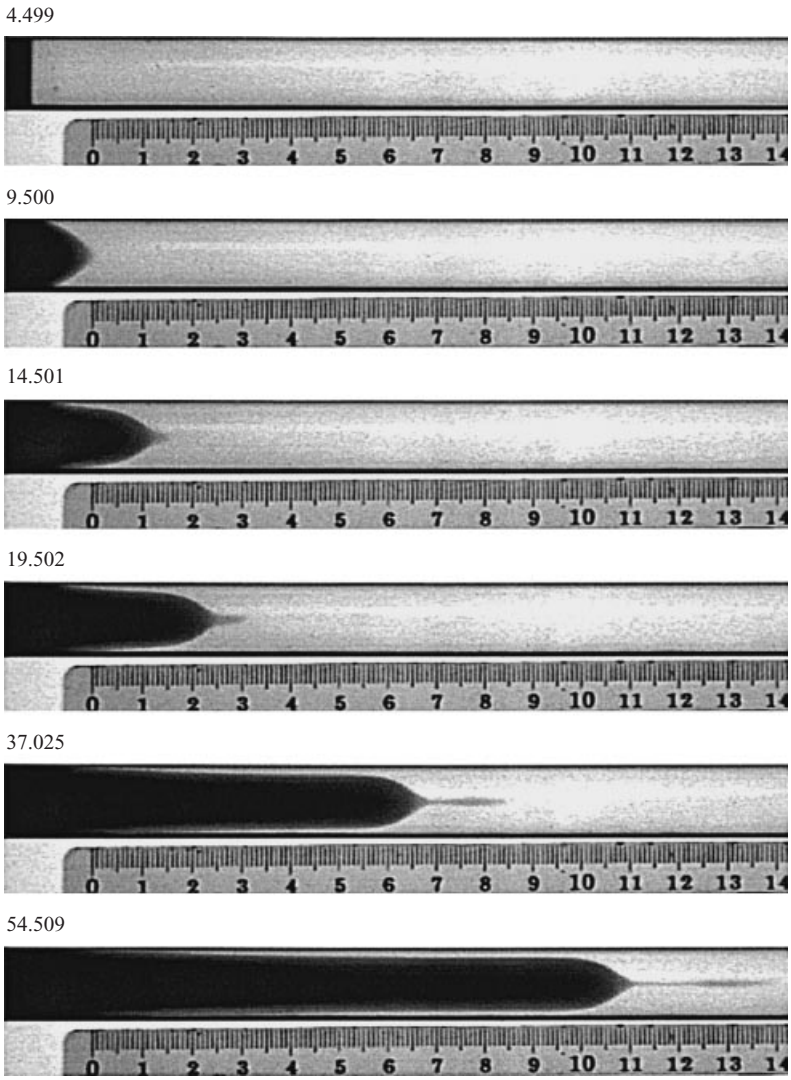


FIGURE 13. Snapshots of miscible displacement in a vertical tube for $M = 57$ and $U = 0.57 < U_{23}(M) = 0.77$ (domain 2), at different time intervals.

experimental apparatus as in the Hele-Shaw cell problem. Now, the transmitted light intensity satisfies the relation

$$I(x, y) = I_0(x, y)\mathrm{e}^{-\alpha b\sqrt{\overline{C}(x,t)/\pi}}. \tag{5.4}$$

As in the Hele-Shaw cell case, it was found that the experiments were satisfactorily described by the theory in domains 1 and 2, whereas the agreement was not as good for $M$ and $U$ values corresponding to domain 3.

This is illustrated in figure 14 (see also figure 12), which shows typical experimental and calculated velocity profiles $V(\overline{C})$ for $M = 23.9 > M_3^{\min}$ and for two flow rates, below and above $U_{23}(23.9) = 0.86$, respectively. On 14($a$), it is seen that, as predicted for domain 2, the distance between the trailing shock and the leading tip increases with time. This is consistent with the observations of Petitjeans & Maxworthy (1996),

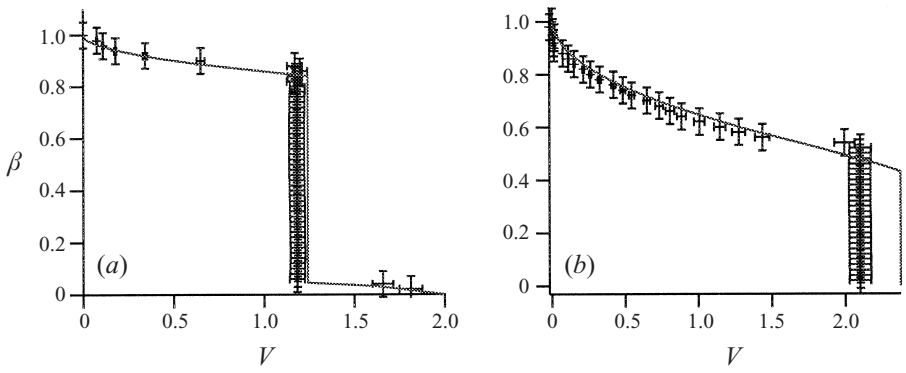


FIGURE 14. Comparison between experimental (symbols) and theoretical (solid line) velocity profiles in a tube for $M = 23.9$, $U = 0.15 < U_{23} = 0.86$ ($a$) and $U = 1.23 > U_{23}$ ($b$). The profiles are given as functions of $\beta = \sqrt{\overline{C}}$.

who also reported such a growing tip in their experiments in a tube performed at a constant pressure drop. Although their results cannot be directly compared to our theoretical predictions (which are valid for a constant injection rate), it is most likely that the regime they termed 'unsteady' falls in domain 2 of our experiments, where the profile includes a leading self-spreading foot. The agreement with the theory (based on contact shocks) becomes poorer for the case where the profile is in domain 3 ($U > U_{23}(M)$, figure 14$b$), however. The variation of the shock velocity, $V_S$, and the normalized radius, $\beta_M$, corresponding to the upper limiting value $\overline{C}_M$ of the shock, is shown in figure 15 as a function of $U$ for $M = 23.9$. Here, the experimental value for the shock strength is larger, while its velocity is smaller, than expected from the theory (of course, the theory does predict the correct velocity, $V_S$, given the correct shock strength). In particular, it appears that in the region $U_{23} < U < U_T$, the front velocity remains close to $V_0$. This disagreement is analogous to the case in the Hele-Shaw cell and was also noted in the non-buoyant case (Chen & Meiburg 1996; Yang & Yortsos 1997; Rakotomalala *et al.* 1997). The notable difference is that, here, an axisymmetric two-dimensional finger is obtained in the entire domain 3, as opposed to the Hele-Shaw cell case, where a three-dimensional pattern emerges at $U > U_T$.

The experimental results for the displacement in the tube are also summarized in the $(M, U)$-plane of figure 12. As in the case of the Hele-Shaw cell, quantitative agreement (filled symbols) was found between experimental profiles and kinematic wave predictions in both domains 1 and 2. The unsteady regime in a tube reported by Chen & Meiburg (1996) falls again in domain 2 (stars). The open symbols correspond to domain 3 and the two cases where the experiments deviate from the theoretical predictions: profiles with a tiny foot and $V_S < V_0$ in domain 3 (open triangles) and profiles exhibiting the qualitative features of domain 3, but with a shock velocity still lower than the expected one (open squares at higher flow rates). Further work is being conducted to understand this deviation.

## 6. Conclusions

In this paper, we studied the vertical displacement, at a constant injection rate $q$, of a viscous fluid by another miscible fluid (with the light fluid injected on top of the heavier one) in the gap of a Hele-Shaw cell or in a tube, and in the high Péclet

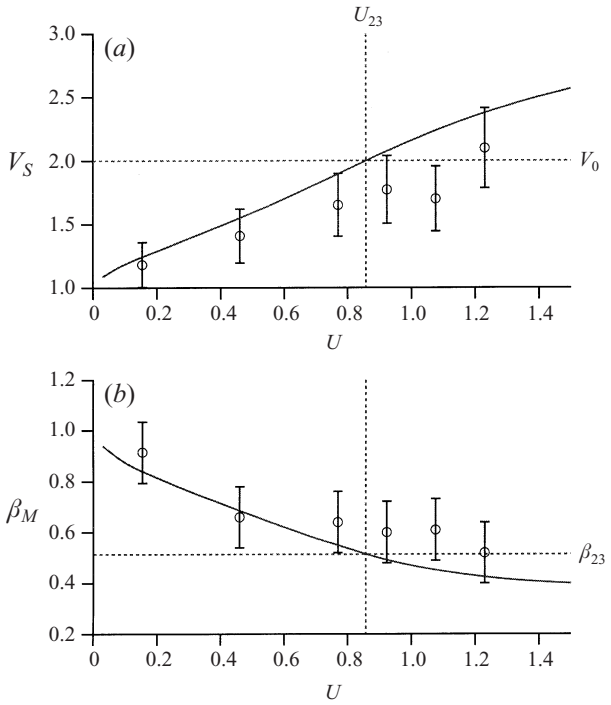


FIGURE 15. Comparison between experimental (circles) and theoretical (solid line) shock velocity $V_S(U)$ (*a*) and the corresponding reduced radius $\beta_M(U)$ (*b*), in a tube, for $M = 23.9$. The theoretical values at $U_{23}$ are indicated by dashed lines.

number regime. The developing tongue was found to be invariant along the width of the Hele-Shaw cell for all rates if the viscosity ratio is sufficiently small, $M < M_T$, and for rates satisfying the condition $U < U_T(M)$, if $M > M_T$. The tongue was always axisymmetric in the experiments in the cylindrical tube. We described the shape of these two-dimensional interfaces, by including buoyancy effects in the kinematic wave approach of Yang & Yortsos (1997). The agreement with the experiments is good, provided that $M < M_3^{\min}$ or $U < U_{23}(M)$, where $M_3^{\min} = 1.5$ and $U_{23}(M)$ is analytically expressed in the case of a Hele-Shaw cell, and $M_3^{\min} = 2$ and $U_{23}(M)$ has to be numerically computed in the case of a tube. In particular, two types of concentration profiles (tongue shapes) observed in the experiments, and separated in the $(M, U)$-plane by a boundary $U_{12}(M)$, are well reproduced by the two-dimensional analysis: self-spreading profiles, and profiles involving an internal shock propagating at a velocity $V_S < V_0$, where $V_0$ is the maximum Poiseuille velocity for single-phase flow ($V_0 = 1.5$ in the cell and 2 in the tube). In the latter case, the shock is preceded by a self-spreading foot already observed in tube experiments by Petitjeans & Maxworthy (1996), and in simulations of miscible flows in a tube and in a Hele-Shaw cell by Chen & Meiburg (1996). On the other hand, for $U > U_{23}(M)$, the theoretical profiles derived from the kinematic wave theory (under the assumption of a contact shock) do not correctly describe the experimental observations: while the theory predicts a contact shock without a preceding tip, travelling at $V_S > V_0$, the measured tongue is wider and slower than predicted, while the front velocity is close to $V_0$. In the Hele-Shaw cell case, the two-dimensional flow pattern destabilizes for sufficiently high flow rates,

giving rise to a three-dimensional fingering instability. The experimental threshold $U_T(M)$ is higher than $U_{23}(M)$, although the threshold $M_T$ is comparable to $M_3^{\min}$.

Y. C. Y. acknowledges the support of DOE Contract DE-FG22-96BC1994/SUB and the hospitality of Universities Paris VI and Paris XI, during the summer of 1997, when part of this work was conducted. The authors also acknowledge NATO grant CRG 973049. The constructive comments of an anonymous referee are also gratefully acknowledged.

## REFERENCES

Bretherton, F. P. 1961 The motion of long bubbles in tubes. *J. Fluid Mech.* **10**, 166–188.

Chen, C. Y. & Meiburg, E. 1996 Miscible displacements in capillary tubes. Part 2. Numerical simulations. *J. Fluid Mech.* **326**, 57–90.

Homsy, G. M. 1987 Viscous fingering in porous media. *Ann. Rev. Fluid Mech.* **19**, 271–311.

Jeffrey, A. 1976 *Quasilinear Hyperbolic Systems and Waves.* Pitman, London.

Lajeunesse, E., Martin, J., Rakotomalala, N. & Salin, D. 1997 3D instability of miscible displacement in a Hele-Shaw cell. *Phys. Rev. Lett.* **79**, 5254–5257.

Manickam, O. & Homsy, G. M. 1995 Fingering instabilities in vertical miscible displacement flows in porous media. *J. Fluid Mech* **288**, 75–102.

McCloud, K. V. & Maher, J. V. 1995 Experimental perturbations to Saffman–Taylor flow. *Phys. Rep.* **260** (3), 141–185.

Park, C.-W. & Homsy, G. M. 1984 Two-phase displacement in Hele-Shaw cells: theory. *J. Fluid Mech.* **139**, 291–308.

Paterson, L. 1985 Fingering with miscible fluids in a Hele-Shaw cell. *Phys. Fluids* **28**, 26–30.

Petitjeans, P. & Maxworthy, T. 1996 Miscible displacements in capillary tubes. Part 1. Experiments. *J. Fluid Mech.* **326**, 37–56.

Rabaud, M., Couder, Y. & Gérard, N. 1988 Dynamics and stability of anomalous Saffman–Taylor fingers. *Phys. Rev.* A **37**, 935–947.

Rakotomalala, N., Salin, D. & Watzky, P. 1997 Miscible displacement between two parallel plates: BGK lattice gas simulations. *J. Fluid Mech.* **338**, 277–297.

Reinelt, D. A. & Saffman, P. G. 1985 The penetration of a finger into a viscous fluid in a channel and tube. *SIAM J. Sci. Statist. Comput.* **6**, 542–561.

Saffman, P. G. & Taylor, G. I. 1958 The penetration of a fluid into a porous medium or Hele-Shaw cell containing a more viscous liquid. *Proc. R. Soc. Lond.* A **245**, 312–329.

Snyder, D. & Tait, S. 1998 A flow-front instability in viscous gravity currents. *J. Fluid Mech.* **369**, 1–21.

Sommerfeld, A. 1954 *Optics, Lectures on Theoretical Physics IV*. Academic.

Tabeling, P., Zocchi, G. & Libchaber, A. 1987 An experimental study of the Saffman–Taylor instability. *J. Fluid Mech.* **177**, 67–82.

Whitham, G. B. 1974 *Linear and Nonlinear Waves.* Wiley-Interscience.

Wooding, R. A. 1969 Growth of fingers at an unstable diffusing interface in a porous medium or Hele-Shaw cell. *J. Fluid Mech.* **39**, 477–495.

Yang, Z. 1995 Application of transverse flow equilibrium in miscible displacements. PhD thesis, University of Southern California.

Yang, Z. & Yortsos, Y. C. 1997 Asymptotic solutions of miscible displacements in geometries of large aspect ratio. *Phys. Fluids* **9**, 286–298.

Zimmerman, W. B. & Homsy, G. M. 1991 Nonlinear viscous fingering in miscible displacement with anisotropic dispersion. *Phys. Fluids* A **3**, 1859–1872.